

# Aeolian sand transport and deposition patterns within a large woody debris matrix fronting a foredune

Michael J. Grilliot <sup>a,b,\*</sup>, Ian J. Walker <sup>c,b</sup>, Bernard O. Bauer <sup>d,b</sup>



<sup>a</sup> Dept. of Geog., University of Victoria, Victoria, BC V8P 5C2, Canada

<sup>b</sup> Hakai Institute, PO Box 309, Heriot Bay, BC V0P 1H0, Canada

<sup>c</sup> School of Geographical Sciences & Urban Planning & School of Earth & Space Exploration, Arizona State University, Tempe, AZ, USA

<sup>d</sup> Earth, Environmental and Geographic Sciences, The University of British Columbia | Okanagan, Kelowna, BC V1V 1V7, Canada

## ARTICLE INFO

### Article history:

Received 2 October 2018

Received in revised form 9 April 2019

Accepted 10 April 2019

Available online 12 April 2019

### Keywords:

Beach-dune systems

Sediment transport

Coastal erosion

Roughness elements

## ABSTRACT

Sediment transport pathways and resulting erosion-deposition patterns across beach-foredune systems can be complex. Although a great deal is known about the effects of wind fetch, surface moisture, topographic forcing, and vegetation cover, the role of large woody debris (LWD) as a control on sediment redistribution across beaches is relatively understudied. Pieces of LWD act as non-porous roughness elements that induce secondary flow circulation, thereby creating unique sedimentation patterns that differ markedly from those over a flat beach. Large accumulations of LWD collectively have a bulk porosity that provides substantial sand trapping volume, yet, no studies to date have quantified the effect of LWD on aeolian sand transport. Results from a field study on a macrotidal beach on Calvert Island, British Columbia, Canada, show that the LWD matrix alters the character of the turbulent boundary layer in a way that reduces sediment flux by 99%. Sand is trapped within the LWD matrix, thereby interrupting sediment delivery from the nearshore to the foredune. As such, LWD has the potential to modulate rates of foredune recovery, growth, and evolution. The relative importance of this effect depends on the density and arrangement of LWD as a fundamental control on aeolian sediment transport, as well as on the magnitude and frequency of events that erode the beach periodically and re-organize the LWD matrix.

© 2019 Elsevier B.V. All rights reserved.

## 1. Introduction

Roughness elements on beaches and coastal dunes (i.e., vegetation, beach wrack, large woody debris) play an important role in beach-dune morphodynamics by acting as an accretion anchor for aeolian sediment, modulating sand transport to foredunes, and providing substrate for incipient dune development (Walker and Barrie, 2006; Nordstrom et al., 2007, 2011; Heathfield and Walker, 2011; Bauer et al., 2013; Eamer and Walker, 2013; Hesp and Walker, 2013). Porous vegetation, for example, has been identified as a key control on sedimentation patterns and foredune growth because the enhanced roughness extracts momentum from wind and induces deposition (Hesp, 1989; Wolfe and Nickling, 1993; Arens, 1996; Hesp and Walker, 2013; Gillies et al., 2014; Keijser et al., 2015; Hesp et al., 2016). Large Woody Debris (LWD), in contrast, is a non-porous roughness element that is relatively understudied in coastal sand transport and sedimentation research (Walker and Barrie, 2006; Eamer and Walker, 2010). This paper addresses this knowledge gap by exploring the geomorphic role of LWD on beach-dune sediment transport.

A LWD matrix is a collection of solid roughness elements arranged in an array with a density that depends on the packing and arrangement of the LWD elements, analogous to other solid roughness arrays (Lancaster and Baas, 1998; Gillies et al., 2006, 2007, 2015; Gillies and Lancaster, 2013). Variations in LWD size, shape, structure, density, apparent porosity, orientation to incoming air flow, and height above the surface create complex flow-form interactions that alter aeolian sediment transport pathways in sometimes unpredictable ways (See Fig. 1). Unlike sand fences, which are linear 2D forms that have been studied extensively (Hotta and Horikawa, 1990; Li and Sherman, 2015; Gillies et al., 2017), LWD matrices are three-dimensional roughness arrays with varying porosity and accommodation space for sediment deposition about which relatively little is known.

LWD is acted upon by littoral and aeolian processes that change its function in the coastal backshore environment. Kennedy and Woods (2012) found that the presence of LWD on gravel beaches helped dissipate wave energy, resulting in gravel deposition in the LWD matrix that led to taller and steeper storm berms. Some studies noted that LWD could be rafted during high water events and act like battering rams to expose more dune area to erosion by ripping up berm and foredune deposits (Stembridge, 1979; Finlayson, 2006; Johannessen and MacLennan, 2007; Heathfield and Walker, 2015). Aeolian accretion within a LWD matrix was identified as key to several geomorphic

\* Corresponding author.

E-mail address: [Grilliot@uvic.ca](mailto:Grilliot@uvic.ca) (M.J. Grilliot).

roles, including damming backshore rivers to create ephemeral pond systems, helping rebuild eroded dune sediment by trapping and storing sediment to be reworked during high water levels, and acting as a nuclei for vegetation establishment and incipient dune formation (Komar and Rea, 1976; Walker and Barrie, 2006; Eamer and Walker, 2010). While every possible function is compelling in its own right, there is a clear knowledge gap in quantifying the impact that a LWD matrix, as a whole, can have on aeolian sand transport and deposition to a coastal foredune (Gonor et al., 1988; Walker and Barrie, 2006; Eamer and Walker, 2013).

The purpose of this study was to identify the effects of a recently reworked LWD matrix on aeolian sand transport and deposition on a high energy, macro-tidal beach. The results from a short-term sediment transport experiment comprising several individual events are placed in the context of seasonal measurements quantifying long-term, post-event volumetric and morphological changes using terrestrial laser scanning (TLS). Sediment transport during a typical transporting wind event was measured along shore-perpendicular transects with varying concentrations of LWD. Event-based sediment transport patterns are linked to alterations to the turbulent boundary layer over the LWD, which were described in a companion paper by Grilliot et al. (2018).

## 2. Methods

### 2.1. Study site

The study site is located on Calvert Island, on the central coast of British Columbia, Canada (Fig. 2). The experiment was conducted on West Beach, a 1-km wide embayed beach bounded by rocky headlands with a SW aspect and relatively open exposure to the Pacific Ocean. The foredune is found on the north end of the beach and is approximately 6.5 m tall and partially vegetated by native dune grass (*Leymus mollis*). The foredune has stoss (seaward) slope angles of 23° to 37° and a crestline orientation of SE–NW (128°–308°). A storm on 10 March 2016, incised the foredune toe creating a 1 to 2 m high scarp that remained near vertical with some slump blocks at the time of the experiment. The beach is macro-tidal with a spring tide range of >4 m, a low tide width of 250 m, and an effective fetch >500 m in the obliquely

alongshore resultant sand drift direction. Data from a nearby meteorological station for 2012 to 2018 shows prevailing winds from the SE (obliquely alongshore). Median grain size ( $D_{50}$ ) of the beach-dune sediments was 0.198 mm (Eamer, 2017) and the aeolian sand transport potential regime (see Fig. 3 inset) is unimodal with a resultant drift potential (RDP) of 111 vector units (vu) toward a resultant drift direction of 322° as derived using the Fryberger and Dean (1979) model per the approach of Miot da Silva and Hesp (2010).

### 2.2. Experimental methods

The experiment was conducted from 11 to 25 April 2016 along three shore-normal transects that were instrumented and monitored (Fig. 3). Transect 1 (T1) was located through an array of dense LWD; Transect 2 (T2) in sparser LWD; whereas Transect 3 (T3) served as the ‘control’ transect, which was cleared of LWD to 4 m on either side. Eighteen 0.3 m long aluminum erosion pins (6 per transect) were installed along each transect in the same locations relative to the scarp base (negative = landward, on the foredune) at -3.3, -1.3, 1.7, 4.2, 7.7, and 13.7 m (Fig. 4). Boundary layer flow information was measuring coincidentally and discussed in detail by Grilliot et al. (2018).

Hilton-style aeolian sediment traps with a sampling orifice of 4 cm<sup>2</sup> (Hilton et al., 2017) were installed in four vertical arrays on aluminum rods on each transect with sampling heights of 10, 20, 30, 40, and 50 cm at the center of the traps (Fig. 5). The arrays were co-located with laser particle counters (LPCs) to measure sand transport intensity at locations 1–2 and 1–4 (7.7 and 1.7 m seaward of the scarp, respectively) on T1 and 3.7 m and 8.5 m seaward of the scarp on T3 (Fig. 4). The landward T3 trap array location was altered slightly from T1 because of a larger dune ramp and to avoid interference with other instruments. Sediment trap arrays were installed for 5 h from 11:00 to 16:00 on 15 April 2016 only. Trap samples were dried, weighed, and reported as mass flux (kg m<sup>-2</sup> day<sup>-1</sup>) and as a percent of the total mass collected at the coincident Trap 3–1 height.

Sand transport intensity (grain counts s<sup>-1</sup>, hereafter referred to as ‘counts’) was measured using LPCs (Wenglor model YH08PCT8) with 80 mm path lengths and a beam width of 0.6 mm. Each LPC was set to



**Fig. 1.** Photos of LWD deposits on West Beach, Calvert Island, British Columbia, Canada. (a) Partially buried log with up- and down-wind sand ramp; (b) dense matrix of logs; (c) matrix of LWD with near complete aeolian in-filling in front of an established foredune.

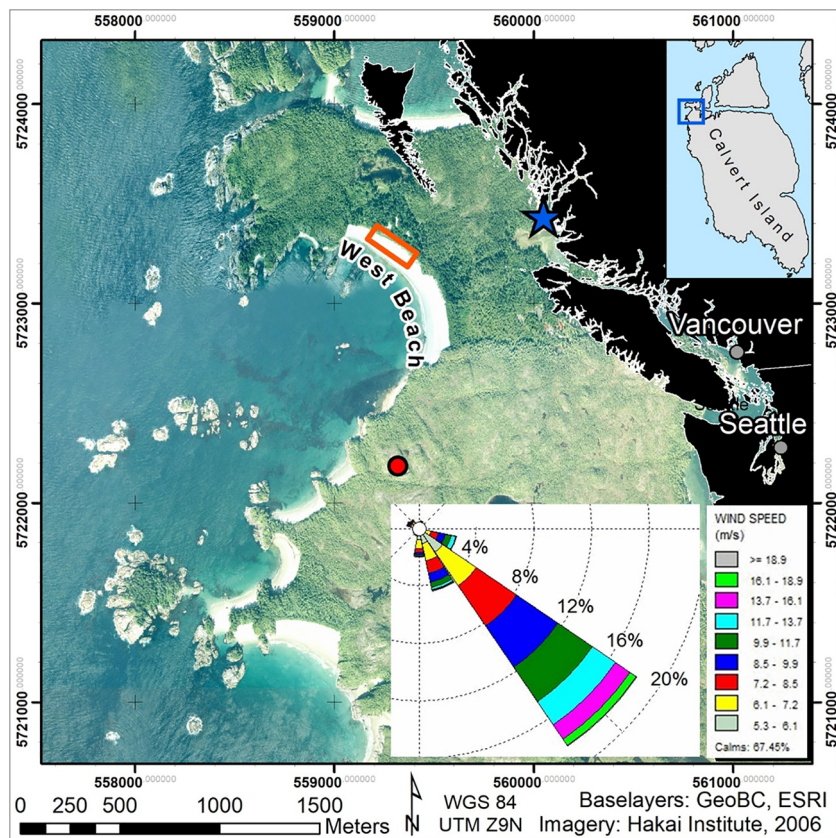


**Fig. 2.** Location of the study area (orange rectangle) on West Beach, Calvert Island, British Columbia, Canada. The red dot shows the location of the weather station used for drift rose calculations (Fig. 3).

(Reproduced from Grilliot et al. (2018) under the Creative Commons attribution license).

the maximum sensitivity, which has the advantage of recording large transport rates (1000 counts per second, i.e., Hz) before significant increases in error arise. For further details on LPC operation and performance see Barchyn et al., 2014; Hugenholtz and Barchyn, 2011; and Bauer et al., 2018. LPCs were placed with the laser sampling beam 0.031 m above the sand surface. Transport directions were variable within the LWD matrix and no cosine adjustments were applied to adjust for wind angle variations relative to the path length of the laser beam. Although these sensors were aligned approximately perpendicular to the incoming wind, count data should be interpreted as relative transport intensity only.

LPCs were hard-wired to Onset® EnergyPro Data Loggers housed in weather-resistant cases. Each data logger had six analog channels for recording anemometer outputs and six digital pulse channels to record LPC counts. All data were sampled and recorded at 1 Hz. Standard data conversion routines were applied following manufacturers' guidelines. Care was taken to clean LPC lenses throughout the day and between runs to reduce moisture and dust contamination.

Surface elevation change measurements were collected at five seasonal intervals (Apr 2016, Jul 2016, Sep 2016, Apr 2017, Aug 2017) using a Riegl VZ-1000 TLS with a precision of 8 mm at 100 m distance. Environmental conditions (visibility, temperature, relative humidity, and barometric pressure) are parameterized on the scanner during the time of measurement to account for atmospheric variability in scan accuracy (Wang et al., 2014; Fabbri et al., 2017). Post-processing was completed in RiScan Pro© software. Individual scan positions were initially registered using stationary targets (10 cm diameter cylindrical reflectors) sited over benchmarks or using a top-mounted Trimble R10 GNSS receiver in Real Time Kinematic (RTK) mode linked to a network-surveyed base station. Individual scan registration was refined

using the Multi-Station Adjustment (MSA) tool in RiScan Pro that matches similar points and features between scans to improve accuracy. Relative registration of all scans to the July 2016 survey was completed to eliminate possible GNSS errors and the need for repeat RTK ground-truthing surveys. Final registration accuracy for each survey date was  $<1$  cm RMSE. Vegetation and LWD were removed from the TLS point clouds using the vegetation filter in RiScan Pro and an iterative refinement method developed by Riegl (2010). A conservative absolute accuracy for each survey was set at 2 cm to account for potential inaccuracies associated with vegetation and LWD removal for digital terrain model (DTM) creation. DTMs were created in Quick Terrain Modeler (QTM) version 8.0.7 using adaptive triangulation at 5 cm<sup>2</sup> raster size. Volumetric analysis was performed in Geomorphic Change Detection (GCD) 7.0 software plugin for ArcGIS (Wheaton et al., 2010) using the spatially uniform student's *t*-test to determine significant volumetric change (*p*-value of 0.05).

To monitor geomorphic changes to the beach and dune between volumetric surveys a RECONYX™ HC500 HyperFire™ camera was installed on the dune (location shown in Fig. 3) looking west-northwest. Images were taken every 15 min from 7 am to 7 pm local time.

### 3. Results

#### 3.1. Transport processes

Sand transport events considered in this study represent a subset of eight 10-min runs from the 13 and 15 of April 2016 (Fig. 6). Transport was highly intermittent during the experiment and only those periods with significant transport activity and limited directional deviation in the wind field were selected for analysis. Due to limited data logger

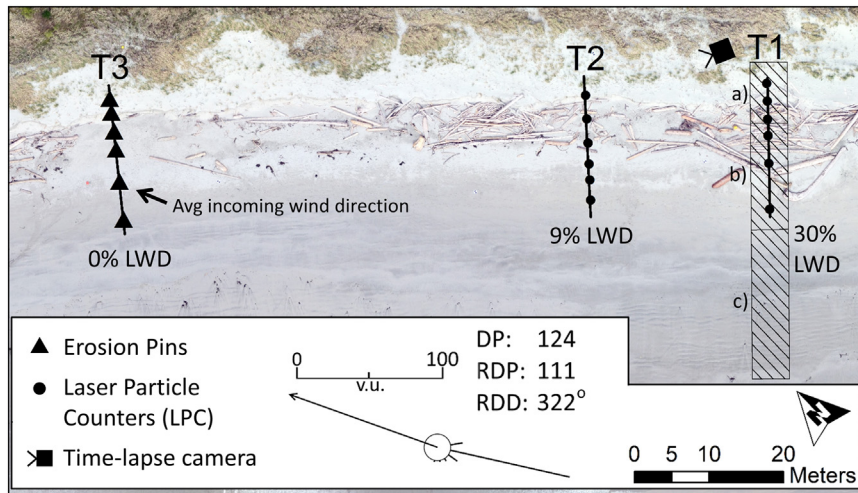


**Fig. 3.** Aerial photograph (11 April 2018) showing the location of transects 1 through 3 (T1–T3) as black lines. T3 is the control transect with minimal LWD cover. The hashed rectangles show the location of the TLS morphological units a) foredune ( $37 \text{ m}^2$ ), b) backshore ( $71 \text{ m}^2$ ), c) foreshore ( $100 \text{ m}^2$ ). The black dots on T1 and T2 show the locations of LPCs. No LPCs were installed along T3. Erosion pins were installed on all transects at the same relative locations as on T3.

capacity, LPC counts were collected only along T1 on 15 April 2016 and only along T2 on 13 April 2016, although both days had similar wind conditions. Raw LPC counts were compared directly and also using an

Activity Parameter that defines the proportion of time in a sampling interval that active transport is recorded (Davidson-Arnott et al., 2012; Smyth et al., 2014). An Activity Parameter value of zero reflects no

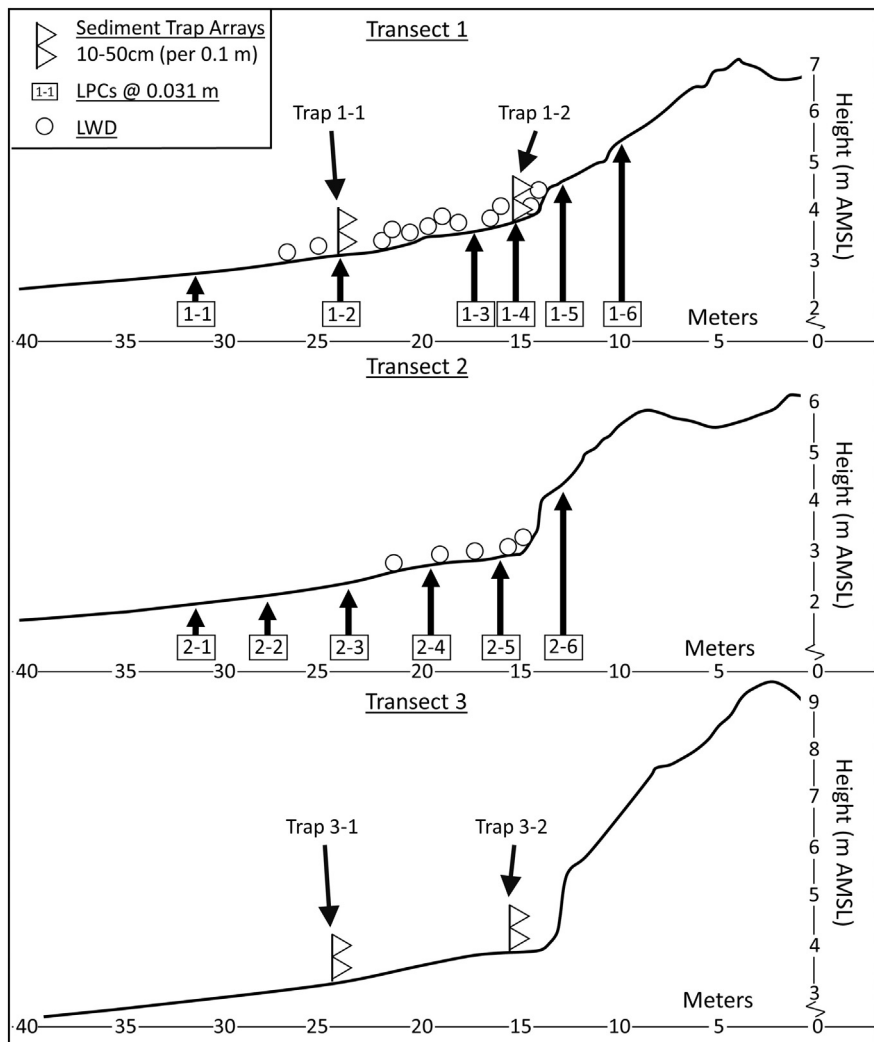


**Fig. 4.** Diagram of instrument locations on transects 1 through 3. LPCs and sediment trap arrays are named by transect # and closest seaward position (e.g., LPC 2-4 is on T2 and is the fourth sensor from the seaward-most sensor).

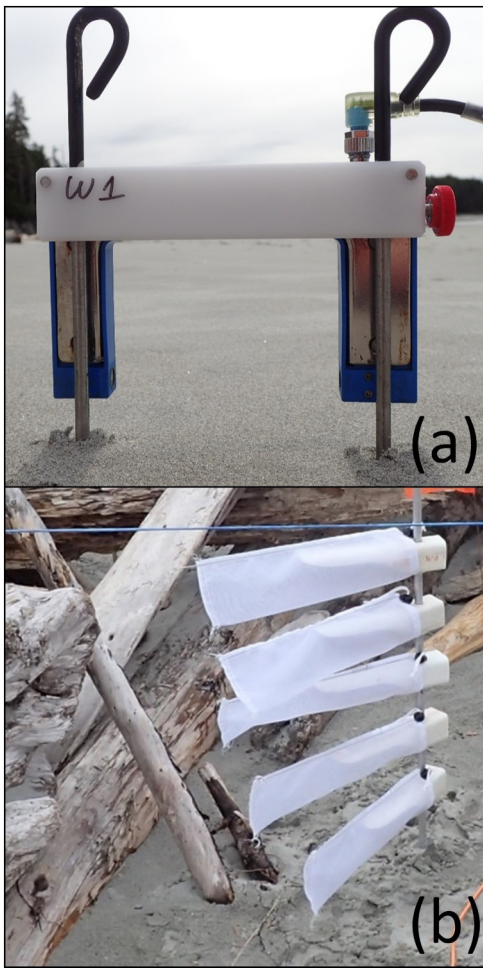


**Fig. 5.** (a) Wenglor LPC, and (b) Hilton-style sediment trap array (Hilton et al., 2017).

transport recorded while a value of one reflects sediment transport in all of the records of the sampling interval. This is the inverse of the intermittency parameter proposed by Stout and Zobeck (1997).

LWD had a clear and measurable effect on sediment transport processes across the backshore. Absolute particle counts and the Activity Parameters downwind of the LWD were much smaller than the unimpeded transport across the beach during all runs (Tables 1 and 2; Fig. 7). LPC counts were reduced by at least an order of magnitude at the first sensor inside the LWD matrix (LPC1-2 on T1; LPC2-4 on T2). The decline in counts was maintained onto the stoss slope (LPC1-5 on T1; LPC2-6 on T2) along both transects. The trends in Activity Parameter were similar, with reductions at the first sensor downwind of the LWD, especially along T1 with a more densely packed LWD matrix. The decline in Activity Parameter was maintained onto the stoss slope of the foredune. The sensors below the foredune scarp and on the stoss slope recorded a 99–100% decrease in counts and Activity Parameters relative to the beach. These observations are consistent with other research showing sand transport decreasing with downwind distance in a roughness array (e.g., Gillies and Lancaster, 2013; Gillies et al., 2015).

Along T2 there were three LPCs on the unimpeded beach upwind of the LWD matrix, and they measured a progressive decline in particle counts across the beach. The most likely explanation is that these LPCs were positioned in the lee of the LWD along T1 given the oblique flow directions (Fig. 7d, f). Nevertheless, there was still an abrupt decline in sediment transport between LPC2-3 and LPC2-4, which coincides with the transition from an open sand surface to the LWD matrix. At the landward extent of the LWD (immediately seaward of the foredune scarp),

LPC1-4 and LPC2-5 recorded little to no counts and therefore zero Activity Parameter. The same is true for the stoss slope (LPC1-5, LPC1-6, and LPC2-6), except during runs 7 and 8 when only a few tens of counts were recorded. These comprise <1% of transport observed on the beach for each run.

The sharp decline in counts and Activity Parameters on both transects just downwind of the transition from open beach to LWD (at LPC1-2 and LPC2-4) is attributed to the roughness effect of the LWD matrix on the turbulent boundary layer. Grilliot et al. (2018) demonstrated that there was an abrupt decrease in mean near-surface wind speed, turbulent kinetic energy, and Reynolds shear stress at the transition into the LWD matrix, as well as a flow steering effect that re-orients the incident wind depending on the stacking orientation of the LWD. Differences in LWD coverage and arrangement along T1 and T2 therefore yielded different transport trends. Fig. 7 illustrates how normalized grain counts (counts<sub>N</sub>) and Activity Parameters decreased within the LWD matrix as a function of downwind distance for all eight runs. The decline in counts<sub>N</sub> and Activity Parameters on T2 downwind of the LWD was not as great as on T1 likely because of less LWD surface cover (Fig. 3) as well as the size and arrangement of the LWD immediately upwind of LPC1-2 and LPC2-4.

### 3.2. Sediment flux

Measured sediment flux data from the Hilton-style traps (Fig. 4) are summarized according to transect (T1 and T3) and height above the surface (10, 20, 30, 40, 50 cm) in Table 3. The vertical array of five traps along the control transect (T3) at location 3-1, which was the most seaward position on the unimpeded beach, accounted for 76% of the total mass collected from all traps, at all locations, because of its unobstructed exposure to uniform streamer activity over most of the beach (Fig. 8). Both traps on Transect 3 were in locations that were distant from the influence of LWD, so the reduced transport at location 3-2 relative to 3-1 likely reflects subtle differences in saltation dynamics as wind moved across the beach closer to the dune scarp. The vertical array of traps at location 1-1 (5 m inside the LWD) and 1-2 (12 m inside the LWD) recorded reductions of 89% and 96%, respectively, of the flux trapped along Transect 3 at the same relative location from the scarp. It is reassuring that the LPCs co-located with the Hilton-style traps on Transect 1 showed similar reductions in transport intensity as a proportion of LPC 1-1 on the unimpeded beach (Table 1). Thus, the spatial trends in sediment transport are real rather than due to measurement uncertainty inherent to the manual versus electronic technologies. In general, the trap data indicate that most of the sediment flux moves close to the bed with variable rates of transport higher in the profile. Traps at location 1-1 recorded slightly elevated mass fluxes at the 20–50 cm trap heights compared to the same trap heights at location 3-1. The differences in flux can be attributed to grains rebounding off the LWD, therefore being launched higher into the flow field than might normally be true for streamers. This will depend on the position of the traps relative to the nature of the LWD immediately upwind. In some instances, trap opening may be sheltered completely whereas in other cases the traps will be within highly turbulent wakes and eddy recirculation zones downwind of large logs.

### 3.3. Geomorphic and volumetric changes

Net morphological change was minimal during the transport experiments, and sand surface elevation fluctuations were within the accuracy of measurement of the erosion pins (approximately  $\pm 5$  mm). Transport fluxes were rather small and highly intermittent, which accounts for the small degree of morphologic change during the individual events monitored during the short-term experiments. However, seasonal changes as measured by TLS scans reveal significant morphologic change driven by the relative impacts of aeolian versus nearshore transport activity. Figs. 9–11 suggest that there is a beach-dune erosion and

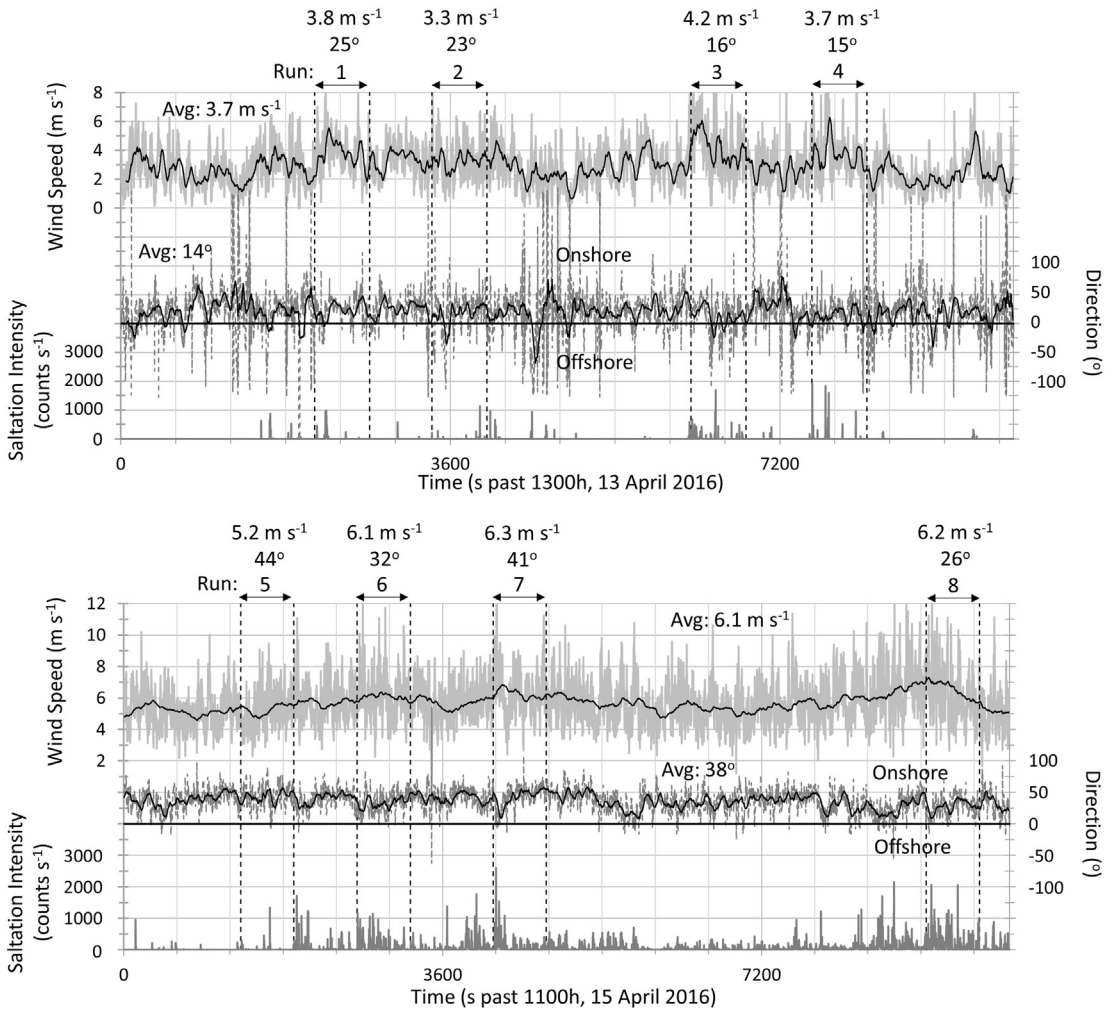


**Fig. 6.** Time series of incident wind speed (upper solid grey line) with 60 s running mean (black solid line) and values indicated by upper left axis ( $\text{m s}^{-1}$ ), wind direction (middle dashed grey line) with 60 s running mean (black solid line) and values indicated by right axis (degrees), and saltation intensity (bottom grey bars) with values indicated along bottom left axis ( $\text{counts s}^{-1}$ ) on 13 April (top graph) and 15 April (bottom graph). Wind speed and direction are from a Gill Instruments 3D sonic anemometer on the beach (7 m seaward of the scarp) on T3 at 1.5 m height. Saltation Intensity is from W1 on T1 (Figs. 4, 5). Selected runs are indicated by the number on the top of each graph with average speed and direction values above. (Reproduced from Grilliot et al., (2018) under the Creative Commons attribution license).

**Table 1**

LPC counts for all 10-min runs. Runs 1–4 were located on T2 and runs 5–8 were located on T1. The transect average of all runs per LPC location is shown normalized as a percent of the LPC 1–1 and 2–1 average respectively (i.e., Average<sub>N</sub>). Cell shading indicates sensor position: no shading shows LPC's seaward (upwind) of the LWD; light gray shading shows LPC's within the LWD matrix, and dark gray shows LPCs on the stoss slope of the foredune. See Fig. 4 for LPC locations relative to the LWD and scarp.

	LPC 1-1	LPC 1-2	LPC 1-3	LPC 1-4	LPC 1-5	LPC 1-6
T1: run 5	7282	24	6	1	3	2
T1: run 6	59811	332	57	1	0	7
T1: run 7	101359	2699	220	60	40	40
T1: run 8	5420	758	45	14	4	44
T1: average <sub>N</sub>	100%	1.71%	0.15%	0.03%	0.02%	0.04%
	LPC 2-1	LPC 2-2	LPC 2-3	LPC 2-4	LPC 2-5	LPC 2-6
T2: run 1	12861	6605	5656	268	0	0
T2: run 2	4394	2404	1682	197	1	0
T2: run 3	24299	14314	8621	488	2	0
T2: run 4	21613	18644	11789	897	2	0
T2: average <sub>N</sub>	100%	66.44%	43.93%	2.93%	0.01%	0.00%

**Table 2**

LPC 10-min activity parameters for all 10-min runs. Runs 1–4 were located on T2 and runs 5–8 were located on T1. The transect average of all runs per LPC location is shown normalized as a percent of the LPC 1–1 and 2–1 average respectively. Cell shading indicates sensor position: see Table 1 for details. See Fig. 4 for LPC locations relative to the LWD and scarp.

	LPC 1-1	LPC 1-2	LPC 1-3	LPC 1-4	LPC 1-5	LPC 1-6
T1: run 5	0.20	0.01	0.01	0.00	0.01	0.00
T1: run 6	0.68	0.12	0.05	0.00	0.00	0.01
T1: run 7	0.65	0.12	0.07	0.03	0.00	0.00
T1: run 8	0.67	0.08	0.02	0.01	0.01	0.02
T1: average <sub>N</sub>	100%	13.2%	6.6%	1.7%	0.9%	1.8%
	LPC 2-1	LPC 2-2	LPC 2-3	LPC 2-4	LPC 2-5	LPC 2-6
T2: run 1	0.13	0.12	0.17	0.08	0.00	0.00
T2: run 2	0.09	0.07	0.09	0.06	0.00	0.00
T2: run 3	0.33	0.28	0.29	0.14	0.00	0.00
T2: run 4	0.18	0.15	0.18	0.11	0.00	0.00
T2: average <sub>N</sub>	100%	83.8%	101.3%	56.2%	1.2%	0.0%

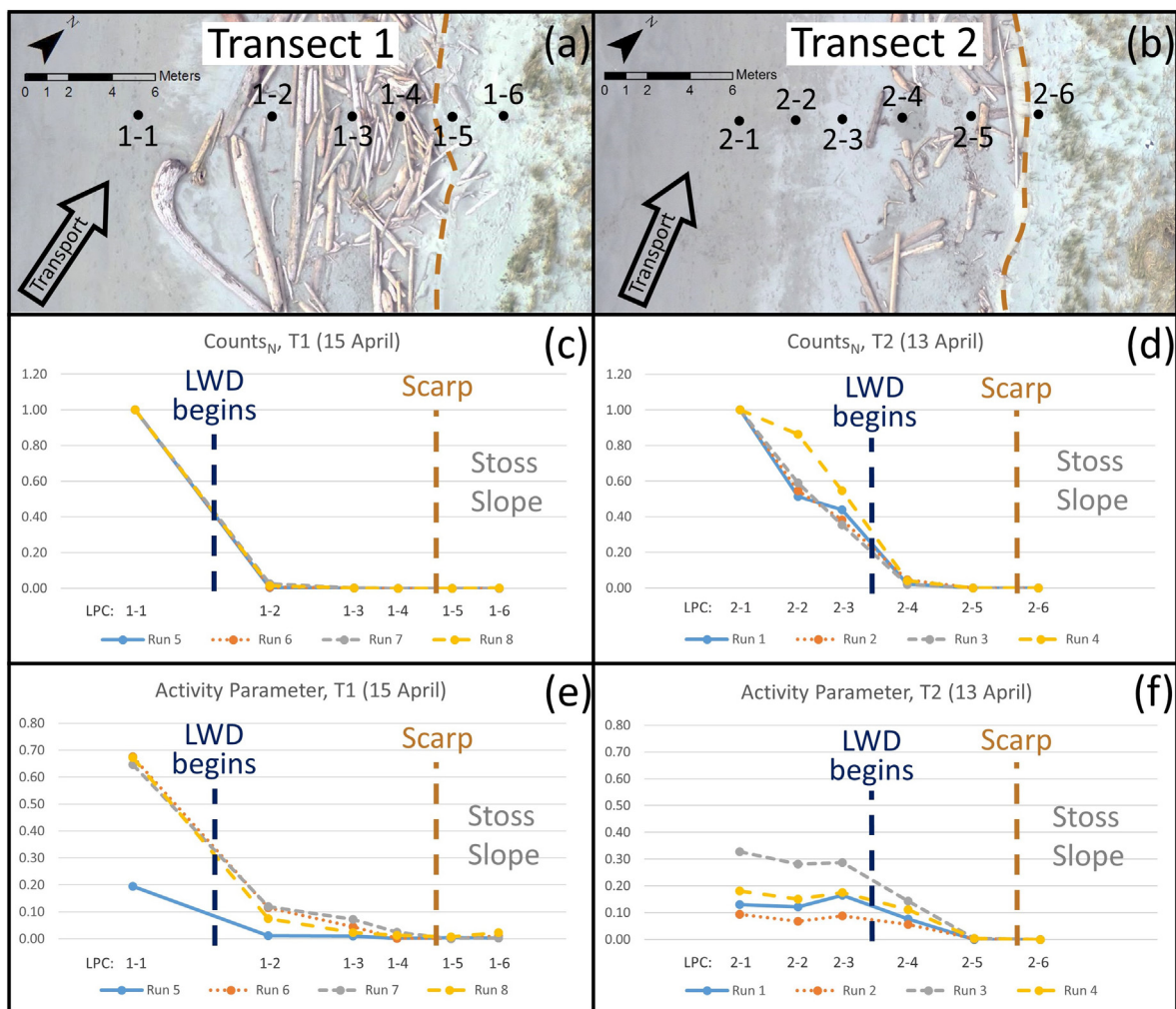


**Fig. 7.** Summary of transport intensity data showing: LPC locations and average incoming wind direction (a, b); counts<sub>N</sub>, which shows the absolute values normalized by LPC 1-1 and 2-1 on each transect (c, d); and 10 min activity parameter (e, f) for runs 5–8 on T1 (a, c, e,) and runs 1–4 on T2 (b, d, f).

rebuilding cycle that mimics the classic summer-winter beach profile model first developed for the beaches of Southern California (Shepard, 1950). The TLS scans show that there was foreshore accretion in the summer (approx. +0.5 m), followed by erosion in the winter (approx. -0.6 m). However, the signal is less clear on West Beach because of the macro-tidal context, which influences the geomorphic effectiveness of storms depending on their timing relative to tidal phases. A major storm may only have a minimal impact on the beach in terms of wave erosion if it occurs during low tide and is short-lived, but this same storm may be accompanied with substantial aeolian redistribution of sediment depending on wind speed and direction.

**Table 3**

Sediment trap mass flux density ( $\text{g m}^{-2} \text{ min}^{-1}$ ). Total sediment trap array (10–50 cm) data are also shown.

Trap height (cm)	T1 (with LWD)		T3 (No LWD)	
	Location 1-1	Location 1-2	Location 3-1	Location 3-2
10	9.38	0.63	156.67	27.92
20	4.17	0.42	1.25	2.29
30	1.67	0.21	0.00	0.21
40	1.25	0.00	0.63	0.42
50	1.67	0.00	0.21	0.21
Total	18.13	1.25	158.75	31.04

Following a major wave event in March 2016 that scarped the foredune, minor readjustments on the scarp face and lower foredune slope were evident by April 2016 in the form of block slumping and grain fall deposits at the base of the scarp (Fig. 12). Fig. 10 shows that erosion of the dune decreased over time as the sand ramp fronting the foredune redeveloped.

From April to Sept 2016, wave-deposited sediments on the foreshore and backshore partially buried some of the LWD by an average of 0.4 m (Fig. 10, profile A-A' and Fig. 11a). As the beach aggraded and the storm season subsided, wave runup events became less effective in reaching the backbeach zone, leaving it exposed to aeolian transport dominance. However, generally calm winds during this period resulted in only minor aeolian accretion (Fig. 9). Even so, the detail shown in Fig. 11 shows localized aeolian deposits occurring as small sand ramps on the windward (Fig. 11a) and leeward sides (Fig. 11b) of individual pieces of LWD, reinforcing the importance of the LWD matrix in inducing aeolian sediment deposition.

The Fall and Winter months (September 2016–April 2017) revealed significant aeolian deposition within the LWD matrix, as well as the formation of a fully developed aeolian sand ramp at the base of the foredune (Fig. 11b). The total net change in the backshore LWD was  $0.66 \text{ m}^3 \text{ m}^{-2}$  (Fig. 9). Despite significant rainfall during the fall and winter, aeolian deposition in the LWD matrix zone was pronounced because of increased windiness relative to summer. This created a situation where sediment delivered to the foreshore in the summer, building



**Fig. 8.** – Image showing uniform distribution of streamers on the beach moving toward the observer (looking upwind to the southeast) during run 6 on 15 April 2016.

the beach, occurred during a different season than peak aeolian activity building the dune. Similar findings have been reported on the Pacific coast in Washington State where sediment delivery to the beach by waves is out of phase (occur at different times of the year) with peak aeolian activity to the foredune zone (Cohn et al., 2018).

Time-lapse imagery (Fig. 13) revealed that most of the aeolian deposition in the LWD matrix was largely the result of a single wind storm in early November 2016, which lasted several days. Pre-event conditions are shown in Fig. 13c, whereas post-event conditions are shown in Fig. 13d, indicating complete burial of the LWD matrix (Fig. 11b and c). A

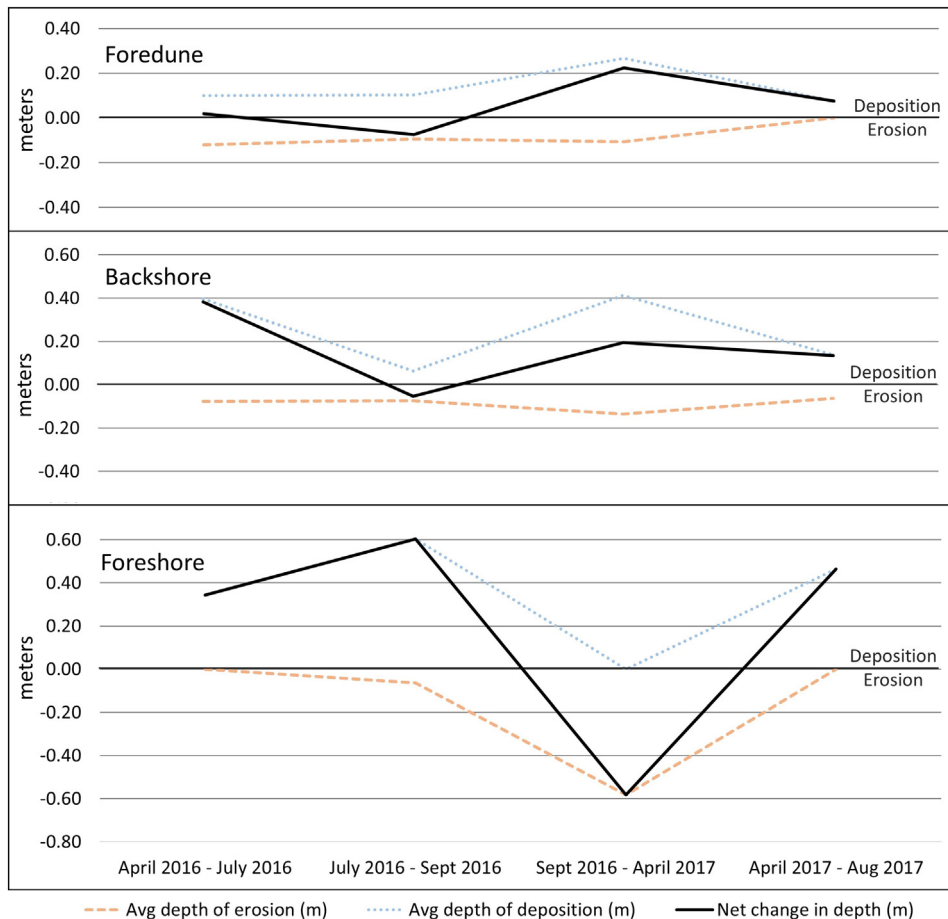


**Fig. 9.** Graphs showing changes in average depths of erosion and deposition during TLS scan intervals for each morphological unit over the area of detectable change (see Fig. 10 for unit areas).

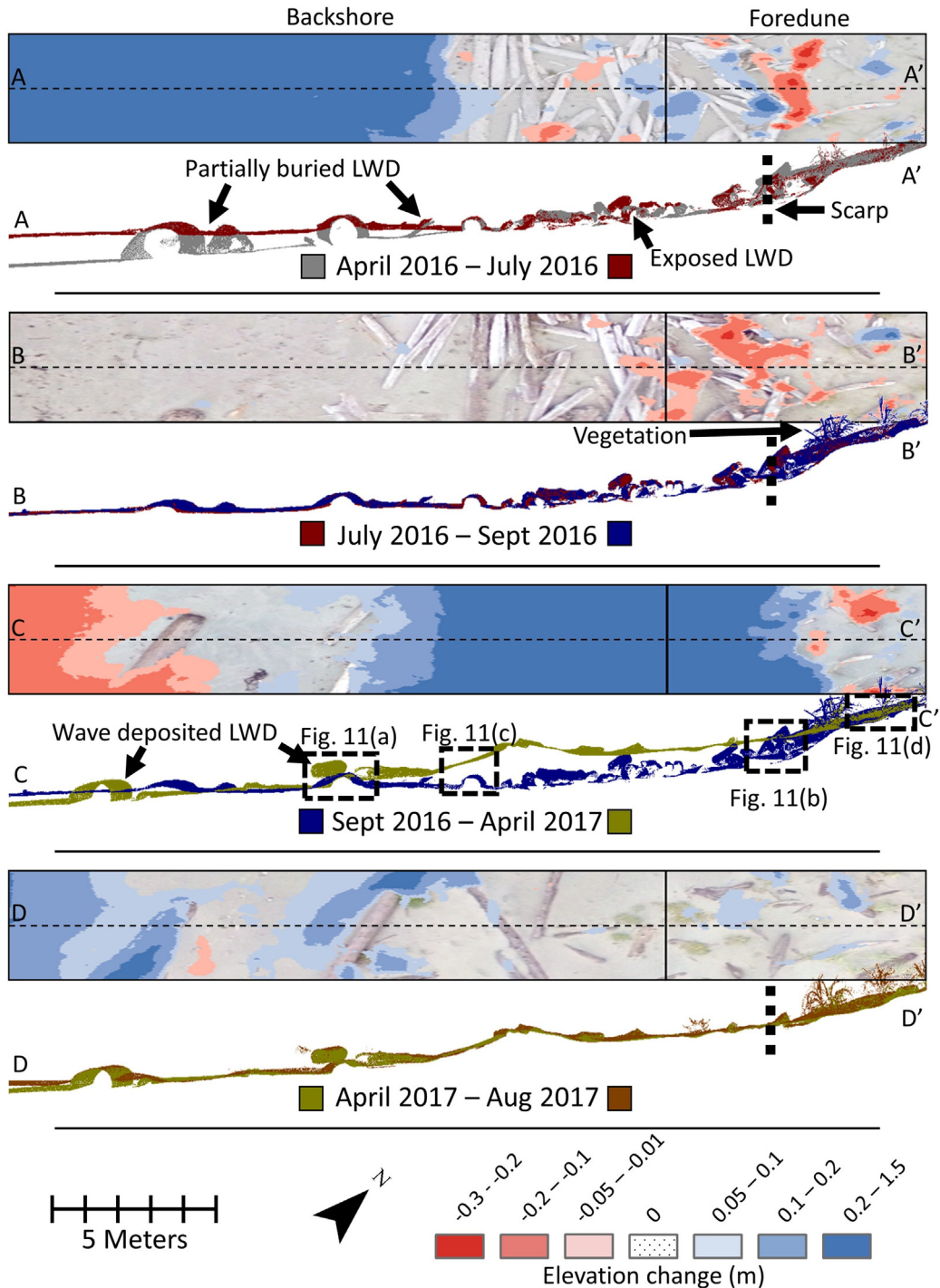


**Fig. 10.** Volumetric and profile changes between TLS surveys in the study area; April 2016–July 2016, July 2016–Sept 2016, Sept 2016–April 2017, and April 2017–Aug 2017. Plan view raster maps: The study area (see Fig. 3 for location) is divided into three morphological units; foreshore (not shown), backshore, and foredune. Significant volumetric changes ( $p = 0.05$ ) to the study area are reported as deposition (blue) and erosion (red), see legend bottom-right. Underlying orthoimagery is from the later date in the date range. Dashed lines indicate the location of the TLS profiles. The short (y) axis of the raster is condensed to fit the figure and is actually 5 m wide. The long (x) axis is to scale, spanning a total beach width of 22.5 m. The foreshore is approximately 20 m in length. Profiles: extracted TLS profiles include points within 1 m on either side of the profile line. Locations of LWD, vegetation, and the scarp are indicated on the figure. The crest of the scarp is 3.7 m AMSL (CGVD28). Dashed rectangles on profile A-A' show locations of the detail in Fig. 11. The profile is to scale with no vertical exaggeration.

later high-water event emplaced newly introduced LWD on top of the aeolian accretion layer (Fig. 10, profile C-C' and Fig. 11a), and a wave-constructed storm berm evolved about 5 m seaward of the scarp. Morphological changes in the summer of 2017 (Fig. 13f) were the same as the summer of 2016 (Fig. 13b) with the foreshore building by swell action and relatively little change on the backshore (no significant aeolian activity, consistent with the wind climatology).

#### 4. Discussion

##### 4.1. LWD as a modulator of aeolian sediment transport and supply to coastal dunes

The short-term transport experiments demonstrate that the LWD matrix was highly effective at trapping sediment moving across the

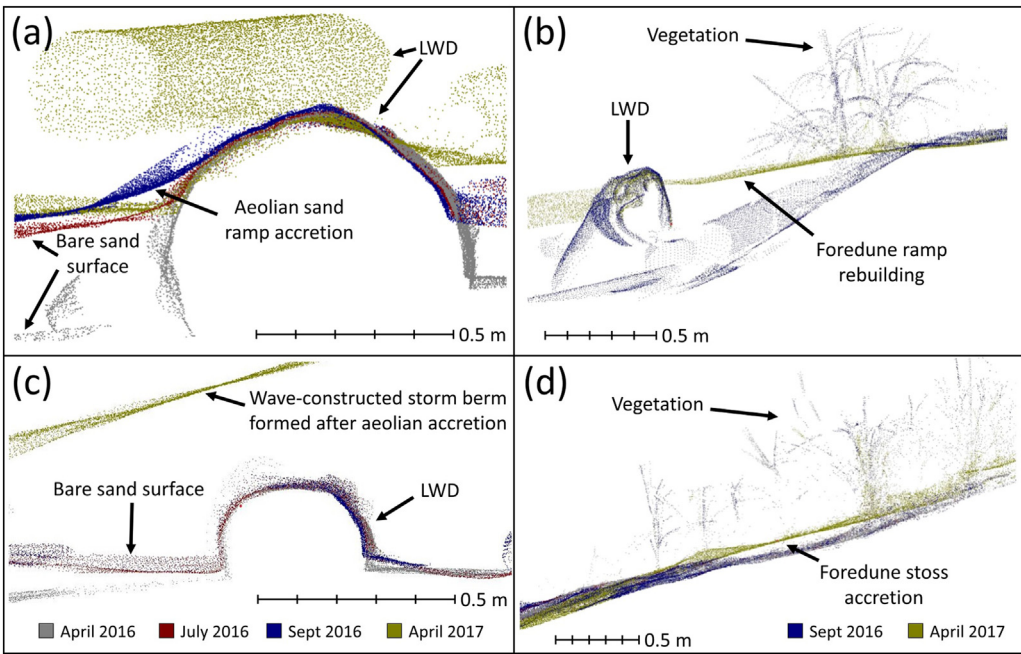


**Fig. 11.** TLS point cloud profiles (1 m wide) showing surface elevation changes between April 2016, July 2016, Sept 2016, and April 2017. (a) shows sand progressively deposited around a large piece of LWD with an additional smaller piece of LWD deposited on top by wave action between Sept 2016 and April 2017. (b) shows the foredune ramp being rebuilt between Sept 2016 and April 2017. (c) shows aeolian deposition around LWD that is eventually buried between Sept 2016 and April 2017. (d) shows minor accretion on the stoss slope amongst vegetation between Sept 2016 and April 2017. Each panels scale is shown while (b) shows the legend for (a) and (b), and (d) shows the legend for (c) and (d).

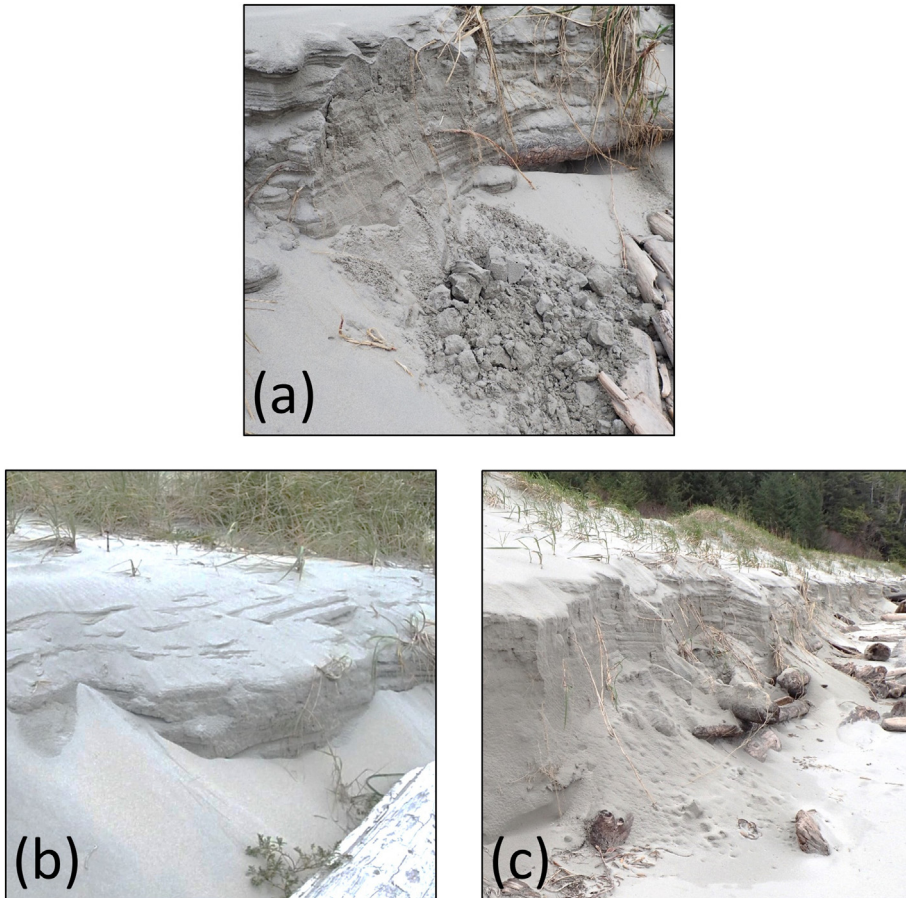


**Fig. 12.** Examples from the study site showing (a) blockfall, (b) grainflows, (c) combination of blockfalls, grainflows, and slumping partially burying LWD and beginning to rebuild the foredune ramp (April 2016).



**Fig. 13.** Images from the time-lapse camera looking WNW (see Fig. 4 for locations). Panels (c) and (d) show before and after a series of active aeolian transport events that bury nearly all of the LWD. Additional wave-deposited LWD can be seen in panel (e) while vegetation colonizes the backshore over the summer months (f).

backshore toward the dune. The sediment trapping potential of LWD therefore can limit the re-supply of sediment to the foredune, especially after a major wave-scarping event has eroded the dune toe. Depending on the degree to which the LWD matrix has been infilled by aeolian deposition, which alters the aerodynamic roughness and boundary layer turbulence (Grilliot et al., 2018), saltating grains moving across the beach might be trapped at the upwind edge of the LWD (when the matrix accommodation space is empty) or continue to move across the LWD matrix (when the accommodation space is full). The seasonal volumetric survey and TLS profiles (Figs. 10 and 11) show examples of all these morphodynamic states because the LWD matrix was progressively in-filled during the seven months of observation. New LWD was deposited atop the former deposit by subsequent storms.

Sand transport and deposition through the matrix decreased with downwind distance from the leading edge. Figs. 14 and 15 illustrate the

relationship between total sand transport counts and normalized downwind distance within the LWD matrix along T1 and T2, respectively. Gillies and Lancaster (2013) and Gillies et al. (2015) suggested that a negative exponential relationship was appropriate for sand transport reductions within a uniform, artificial roughness array. While our data are not directly comparable (because the LPCs in this study were not calibrated to provide mass transport flux), Gillies et al. (2015, Fig. 7,  $R^2 = 0.94$ ) found a similar relationship to the exponential depletion of transport in their uniform array which was located on a flat desert surface. Understanding such decreasing transport trends within a LWD matrix is challenging because the roughness array parameters are irregular and highly complex, unlike the experimentally-emplaced, uniform arrays used by Gillies et al. (2015). The presence of the foredune in altering flow conditions due to pressure effects and topographic steering also complicates matters with natural LWD matrices. Moreover, the

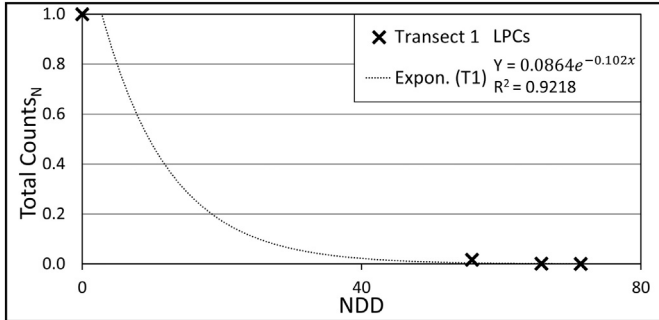


**Fig. 14.** Total counts<sub>N</sub> (defined as the ratio of total grain counts for all runs at a LPC divided by the total grain counts for all runs at the seaward-most LPC per transect) for all runs on Transect 1 as a function of normalized downwind distance (which is defined as the downwind distance from the seaward most LPC divided by the average height of LWD along T1 and T2 (estimated to be 0.25 m from the TLS scans). LPCs 1–4 and 1–5 are excluded as they were on the stoss slope.

relationships are temporally variable because the accommodation spaces within the LWD matrix will infill or empty and typically be re-arranged by high water events, thereby affecting the aerodynamic roughness and trapping efficiency. While it is possible that the differences in T1 and T2 trends are the result of different LWD coverages and/or roughness effects, it is entirely possible that the differences are a statistical anomaly because of the limited number of data points. In either case, further research is required to attribute the physical cause of the differences in regression trends by transect. The relative agreement with Gillies et al. (2015) demonstrates the similarity between complex natural roughness matrices to those that have tighter experimental control.

Despite the enhanced trapping efficiency of a partly filled LWD matrix, there will always be secondary pathways for sediment transport through the zone of LWD, depending on stacking, orientation, and density. Some of these transport corridors are parallel to logs and occasionally underneath logs that are perched on others, where flow can be accelerated through a hollow thereby preventing local deposition. In other instances, grains move over-top the matrix. Although grain suspension was not observed directly during the experiments due to the moderate wind speeds encountered, the 20–50 cm height traps 5 m inside the LWD (Trap 1–1) recorded more sand transport than Trap 3–1 on the unimpeded beach (Table 3). This is likely the result of rebounding sand in modified saltation over the LWD at lower heights, such that these grains bounce higher into the flow field than they normally might in the absence of the LWD. For the events observed in this study, this transport mechanism appears limited to the upwind portions of the LWD matrix as it was not documented 10 m into the LWD matrix (trap 1–2). Grilliot et al. (2018) describe shifts in the character of the turbulent boundary layer during the same event that enhanced shear stress

over the LWD, which could facilitate continuous transport over the LWD. However, the increase in shear stress was accompanied by a marked reduction in mean flow speed and turbulent kinetic energy immediately above the LWD, which explains why the rebounding effect was limited to the upwind section of the LWD zone. Experimentation during faster winds is needed to assess if this mechanism can be maintained across the entire LWD matrix, as suggested by Anderson and Walker (2006).

#### 4.2. Long-term impacts of the LWD matrix on foredune recovery and growth

The long-term impacts of a LWD matrix on a foredune are poorly understood but potentially quite important. A recently deposited matrix of LWD has significant capacity to trap and store sediment, thereby preventing delivery of aeolian sand to the foredune. For example, if a major storm event scars the foredune and emplaces LWD on the backshore, the presence of the LWD matrix will impede the rapid healing of the foredune scarp by aeolian processes. Without a well-developed sand ramp leading to the stoss slope of the foredune, very little sediment can make its way up the stoss slope toward the crest. Not only can the foredune not grow, the crest can be eroded, especially in the absence of a protective cover of vegetation during intense wind events (as experienced in winter). As the accommodation space in the LWD matrix is infilled with sediment that would otherwise reach the foredune, the matrix will gradually lose its ability to impede sediment transport to the foredune. Such decreasing sand capture capacity has been noted for sand fences (Hotta and Horikawa, 1990; Nordstrom et al., 2006, 2007, 2011; Gillies et al., 2017), 3D roughness arrays (Gillies et al., 2015), and beach wrack (Dugan and Hubbard, 2010; Nordstrom et al., 2011).

While beach wrack is also naturally deposited and may play a similar role to LWD, there are a few primary differences between typical wrack deposits and LWD matrices as transport modulators. The wrack deposits, although important to incipient dune formation (Hesp, 2002), are usually of limited height and width with gentle slopes so they do not protrude as aggressively into the boundary layer as does LWD. Grilliot et al., (2018) showed that the LWD matrix increased vertical mixing and reduced wind speed up to 1.5 m above the surface. These effects resulted in decreased transport recorded to a height of 0.5 m in this study. The LWD matrix in this study was also comprised of a complex network of overlapping pieces that was up to 15 m wide and up to 0.5 m high in places. The scale and shape alone make the LWD matrix far more effective at altering airflow and reducing sediment transport than typical beach wrack deposited in shallow shore-parallel ridges or scattered across the beach surface. Admittedly, beach wrack (and other deposits of marine vegetation washed on the shore) has been recorded up to a depth of 0.3 m and sometimes higher, but in these instances there is relatively little accommodation space between the individual plants. Given that a LWD matrix can vary in size and density it seems more appropriate to conceptualize the role of the LWD matrix in this study as having properties similar to the artificial roughness arrays studied by Gillies and Lancaster (2013) and Gillies et al. (2015) rather than typical beach wrack.

A beach-dune system offers the potential for understanding cyclical evolutionary relationships between LWD and sand supply because of the combined effects of nearshore and aeolian processes. Waves and currents can erode the beach and thereby exhume, rework, and redeposit buried LWD, which increases the potential for aeolian sand storage on the beach (Komar and Rea, 1976). The March 2016 erosion event exposed a large amount of previously buried LWD, as indicated by the numerous logs protruding out of the established foredune (Fig. 16). The sediment liberated from within a LWD matrix during high water events could be stored temporarily in the nearshore zone, only to be returned to the foreshore and backshore during swell wave conditions. Thereafter, aeolian transport is essential to moving sand from the foreshore to

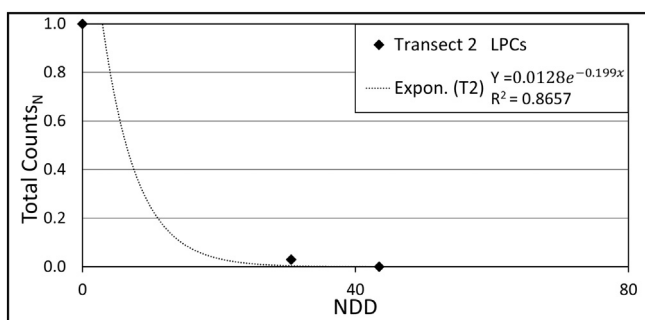


**Fig. 15.** Total counts<sub>N</sub> for all runs per transect 2 as a function of normalized downwind distance. LPCs 2–2 and 2–3 are excluded due to downwind interference from transect 1, as is LPC 2–6 which was on the stoss slope.



**Fig. 16.** Previously buried logs exhumed from within the established foredune after the 10 March 2016 high water storm event. The scarp in the center of the photo is approximately 1.5 m high.



**Fig. 17.** Study site on Calvert Island, British Columbia showing a freshly deposited sand ramp almost reconnecting the upper beach and the foredune stoss slope (May 2017).

the foredune, but this process is mediated by the effectiveness of the LWD matrix in trapping sand moving landward.

The temporal phasing of aeolian activity leading to deposition on the backshore and foredune relative to wave reworking events that mobilize sand and LWD is important because it controls how effective the LWD matrix is as a roughness element and sand trapping reservoir. In turn, this will influence sediment delivery to the foredune, despite a seemingly adequate sediment supply in the littoral cell. This confounds the interpretation of cycles of foredune recovery and growth in relation to from the magnitude and frequency of storm events. For instance, if a LWD matrix is reworked frequently by waves during storms, then the net effect could be to substantially limit sediment supply to the foredune for rebuilding, even if the aeolian system is otherwise very active. On beach-foredune systems without LWD, most of the aeolian sands could contribute immediately to infilling the scarp and building a sand ramp at the base of the foredune with subsequent contributions to the stoss slope (Ollerhead et al., 2013; Davidson-Arnott et al., 2018). However, with an extensive matrix of LWD, aeolian sediments are trapped within the LWD and only a fraction reaches the scarp base. Alternatively, if a LWD matrix is reworked infrequently by waves it will experience infilling by aeolian sediment and gradually cease to be an effective modulator of sand delivery to the foredune. Depositional lobes emanating from the LWD matrix will eventually connect to the foredune scarp and build a sand ramp that re-connects the sediment conveyance from the beach to the stoss slope and beyond. Fig. 17 shows the gradual evolution of the sand ramp from very steep avalanche slopes (with sediment derived from the lower stoss slope of the foredune) to an aeolian accretion deposit connecting the backshore to the scarp face. In the foreground is a scour hollow formed by recirculation eddies at the base of the scarp (Piscioneri et al., 2019). LWD can remain buried under these sediments for extensive periods, not playing any role in the overall morphological adjustments of the beach-dune system until exhumed again by a large storm event, if at all.

Sediments that partially bury the LWD matrix provide a protected site for colonizing vegetation, as evidenced in the Aug 2017 TLS scan (Fig. 10, profile D-D') and time-lapse camera data (Fig. 12f). This evidence supports, in part, the suggested effects of LWD on coastal dune systems identified by Walker and Barrie (2006) and corroborates work by Heathfield and Walker (2011) and Eamer and Walker (2010) on the role of LWD in altering the beach sediment budget. If the accretionary wedge is stabilized by pioneering vegetation, a new incipient dune can evolve that could yield shoreline progradation. Whether this occurs depends largely on the littoral sediment budget (Psuty, 1988).

## 5. Conclusions

The effects of a LWD matrix on aeolian sediment transport potential and subsequent depositional patterns across a beach-dune system were investigated at single wind event and seasonal scales. Sediment traps and laser particle counters were used to quantify transport intensity through the LWD matrix at sampling frequencies of seconds to tens of minutes over a span of hours on multiple days. TLS surveys were spaced many months apart to capture seasonal influences over a span of 16 months. The data were used to investigate resulting erosional and depositional responses of the system to both nearshore and aeolian transporting events. The main findings are:

- LWD had a clear and measurable effect on aeolian sediment transport and acted as a physical barrier to saltating grains moving across the foreshore and toward the foredune. Sediment flux was reduced by 99% at the transition from the unimpeded beach to within the LWD matrix, with most deposition occurring within the first 6 m of the leading edge. The reduced level of transport within the LWD was similar to that found in other research on uniform roughness elements, sand fences, and beach wrack.
- Vertical arrays of integrating sand traps showed that about 97% of saltating grains moved in the surface layer below the average height of the LWD (approximately 0.25 m). However, saltating particles rebounding off the LWD allowed for higher trajectories and farther travel distances than what was measured on a control transect without LWD. It is possible that faster incident wind speeds could facilitate longer particle travel distances and multiple rebounds across the LWD matrix, thereby yielding a direct contribution to the stoss slope of the foredune. But this was not measured during this study due to the slow mean wind speeds. Such an effect likely depends on the width, height, and composition of the LWD matrix as well as the degree to which the accommodation space has been in-filled.
- The LWD matrix in this study reduced sediment transport similar to a uniform roughness array. However, transport reduction varied between different LWD concentrations possibly because of the variations in shape, size, structure, orientation, abundance, exposure, and height above the surface. These variations make modeling the effects of LWD on flow and transport across a foredune difficult. More research is needed to understand the relationship between each possible parameter and its effect on flow and transport over time if LWD is to be included as a natural roughness element in flow models.

- Seasonal TLS surveys indicate that the LWD matrix trapped appreciable amounts of sediment on the backshore ( $0.66 \text{ m}^3 \text{ m}^{-2}$ ). The reduced sand delivery to the foredune could increase the time required to re-build a dune ramp after an erosion event. However, observations at this site show that the LWD can be buried over a matter of days by active aeolian transport, quickly restoring sediment delivery to the base of the foredune.
- The ability for a LWD matrix to trap sediment depends on its effectiveness as a flow modifier and as a physical barrier to sediment transport. These properties change over time depending on the magnitude and frequency of nearshore events that periodically erode the beach and re-organize the LWD matrix. In this way, beach-dune systems adjacent to forested terrain may demonstrate cyclical relationships between LWD, sand supply, and foredune growth. LWD can be exhumed by wind and waves and then in the process of being re-buried by aeolian transport, will limit the sand supply to the foredune. How effective a LWD matrix is at modulating sediment supply to the foredune is related to cycles of foredune erosion and recovery from storm events driven by wave and current action. The synoptic regimes of these events require further study to fully understand the broader geomorphic role of LWD on beach-dune interaction.

## Acknowledgments

This research was conducted in partnership with the Hakai Institute as part of a Coastal Sand Ecosystems research program and was supported financially and logically by partners at the Hakai Institute and Tula Foundation, notably Eric Peterson and Christina Munck. This project was also funded by a Hakai Ph.D. Fellowship to Michael J. Grilliot, Canadian Natural Sciences and Engineering Research Council (NSERC) Discovery grant (no. 239751-2011) and Canada Foundation for Innovation (CFI) Leader's Opportunity Fund (projects #4632 and #29502) to Ian J. Walker. Field assistance was provided by staff from the Hakai Institute and other students from UVic, including Derek Heathfield, Alana Rader, and Felipe Gomez. The authors recognize that this study took place on the traditional territory of the Heiltsuk and Wuikinuxv First Nations, and are grateful for the opportunity. The authors would like to thank the anonymous reviewers whose comments helped improve the manuscript.

## Author contributions

M.J.G., I.J.W., and B.O.B. conceived, designed, and performed the experiments; M.J.G. analyzed the data with guidance from I.J.W. and B.O.B.; I.J.W. and B.O.B. contributed equipment and analysis tools; M.J.G. wrote the first draft of the paper with thematic guidance and editorial assistance from I.J.W. and B.O.B. The Hakai Coastal Sand Ecosystems Program funding was secured by IJW and all site logistics were supported by the Hakai Institute.

## Conflicts of interest

The authors declare no conflict of interest. The founding sponsors had no role in the design of the study; in the collection, analyses, or interpretation of data; in the writing of the manuscript, and in the decision to publish the results.

## References

- Anderson, J.L., Walker, I.J., 2006. Airflow and sand transport variations within a backshore-parabolic dune plain complex: NE Graham Island, British Columbia, Canada. *Geomorphology* 77, 17–34. <https://doi.org/10.1016/j.geomorph.2005.12.008>.
- Arens, S.M., 1996. Patterns of sand transport on vegetated foredunes. *Geomorphology* 17, 339–350.
- Barchyn, T.E., Hugenholtz, C.H., Li, B., Neuman, C.M., Sanderson, S.R., 2014. From particle counts to flux: Wind tunnel testing and calibration of the 'Wenglor' aeolian sediment transport sensor. *Aeolian Res.* 15, 311–318. <https://doi.org/10.1016/j.aeolia.2014.06.009>.
- Bauer, B.O., Walker, I.J., Baas, A.C.W., Jackson, D.W.T., McKenna-Neuman, C., Wiggs, G.F.S., Hesp, P.A., 2013. Critical Reflections on the Coherent Flow Structures Paradigm in Aeolian Geomorphology, in: Venditti, J.G., Best, J.L., Church, M., Hardy, R.J. (Eds.), *Coherent Flow Structures at Earth's Surface*. John Wiley & Sons Ltd., Chichester, West Sussex, UK, pp. 111–134. doi:<https://doi.org/10.1002/9781118527221>
- Bauer, B.O., Davidson-Arnott, R.G.D., Hilton, M.J., Fraser, D., 2018. On the frequency response of a Wenglor particle-counting system for aeolian transport measurements. *Aeolian Res.* 32, 133–140. <https://doi.org/10.1016/j.aeolia.2018.02.008>.
- Cohn, N., Ruggiero, P., de Vries, S., Kaminsky, G.M., 2018. New insights on coastal foredune growth: the relative contributions of marine and aeolian processes. *Geophys. Res. Lett.* 45, 4965–4973. <https://doi.org/10.1029/2018GL077836>.
- Davidson-Arnott, R.G.D., Bauer, B.O., Walker, I.J., Hesp, P.A., Ollerhead, J., Chapman, C., 2012. High-frequency sediment transport responses on a vegetated foredune. *Earth Surf. Process. Landforms* 37, 1227–1241. <https://doi.org/10.1002/esp.3275>.
- Davidson-Arnott, R., Hesp, P., Ollerhead, J., Walker, I., Bauer, B., Delgado-Fernandez, I., Smyth, T., 2018. Sediment budget controls on foredune height: comparing simulation model results with field data. *Earth Surf. Process. Landforms*. <https://doi.org/10.1002/esp.4354>.
- Dugan, J.E., Hubbard, D.M., 2010. Loss of coastal strand habitat in Southern California: the role of beach grooming. *Estuar. Coasts* 33, 67–77. <https://doi.org/10.1007/s12237-009-9239-8>.
- Eamer, J.B.R., 2017. *Reconstruction of the Late Pleistocene and Holocene Geomorphology of Northwest Calvert Island, British Columbia*. University of Victoria.
- Eamer, J.B.R., Walker, I.J., 2010. Quantifying sand storage capacity of large woody debris on beaches using LiDAR. *Geomorphology* 118, 33–47. <https://doi.org/10.1016/j.geomorph.2009.12.006>.
- Eamer, J.B.R., Walker, I.J., 2013. Quantifying spatial and temporal trends in beach-dune volumetric changes using spatial statistics. *Geomorphology* 191, 94–108. <https://doi.org/10.1016/j.geomorph.2013.03.005>.
- Fabbri, S., Giambastiani, B.M.S., Sistilli, F., Scarelli, F., Gabbianelli, G., 2017. Geomorphological analysis and classification of foredune ridges based on Terrestrial Laser Scanning (TLS) technology. *Geomorphology* 295, 436–451. <https://doi.org/10.1016/j.geomorph.2017.08.003>.
- Finlayson, D.P., 2006. *The Geomorphology of Puget Sound Beaches*. University of Washington.
- Fryberger, S.G., Dean, G., 1979. Dune Forms and Wind Regime, in: McKee, E.D. (Ed.), *A Study of Global Sand Seas*, USGS Professional Paper, Vol 1052. US Geological Survey and United States National Aeronautics and Space Administration, Washington D.C., pp. 137–170.
- Gillies, J.A., Lancaster, N., 2013. Large roughness element effects on sand transport, Oceano Dunes, California. *Earth Surf. Process. Landforms* 38, 785–792. <https://doi.org/10.1002/esp.3317>.
- Gillies, J.A., Nickling, W.G., King, J., 2006. Aeolian sediment transport through large patches of roughness in the atmospheric inertial sublayer. *J. Geophys. Res.* 111, F02006. doi:[10.1029/2005F000434](https://doi.org/10.1029/2005F000434).
- Gillies, J.A., Nickling, W.G., King, J., 2007. Shear stress partitioning in large patches of roughness in the atmospheric inertial sublayer. *Boundary-Layer Meteorol.* 122, 367–396. <https://doi.org/10.1007/s10546-006-9105-5>.
- Gillies, J.A., Nield, J.M., Nickling, W.G., 2014. Wind speed and sediment transport recovery in the lee of a vegetated and denuded Nebkha within a Nebkha dune field. *Aeolian Res.* 12, 135–141. <https://doi.org/10.1016/j.aeolia.2013.12.005>.
- Gillies, J.A., Green, H., McCarley-Holder, G., Grimm, S., Howard, C., Barbieri, N., Ono, D., Schade, T., 2015. Using solid element roughness to control sand movement: Keeler Dunes, Keeler, California. *Aeolian Res.* 18, 35–46. <https://doi.org/10.1016/j.aeolia.2015.05.004>.
- Gillies, J.A., Etyemezian, V., Nikolic, G., Click, R., Rowland, P., Pesce, T., Skinner, M., 2017. Effectiveness of an array of porous fences to reduce sand flux: Oceano Dunes, Oceano CA. *J. Wind Eng. Ind. Aerodyn.* 168, 247–259. <https://doi.org/10.1016/j.jweia.2017.06.015>.
- Gonor, J.J., Sedell, J.R., Benner, P.A., 1988. Chapter 4. What We Know About Large Trees in Estuaries, in the Sea, and on Coastal Beaches, in: Maser, C., Terrant, R.F., Trappe, J.M., Franklin, J.F. (Eds.), *From the Forest to the Sea: A Story of Fallen Trees*. U.S. Department of Agriculture, Portland, pp. 83–112.
- Grilliot, M.J., Walker, I.J., Bauer, B.O., 2018. Airflow dynamics over a beach and foredune system with large woody debris. *Geosciences* 8, 147. <https://doi.org/10.3390/geosciences8050147>.
- Heathfield, D.K., Walker, I.J., 2011. Analysis of coastal dune dynamics, shoreline position, and large woody debris at Wickaninnish Bay, Pacific Rim National Park, British Columbia. *Can. J. Earth Sci.* 1198, 1185–1198. <https://doi.org/10.1139/E11-043>.
- Heathfield, D.K., Walker, I.J., 2015. Evolution of a foredune and backshore river complex on a high-energy, drift-aligned beach. *Geomorphology* 248, 440–451. <https://doi.org/10.1016/j.geomorph.2015.08.006>.
- Hesp, P.A., 1989. A review of biological and geomorphological processes involved in the initiation and development of incipient foredunes. In: Gimingham, C.H., Ritchie, W., Willetts, B.B., Willis, A.J. (Eds.), *Coastal Sand Dunes. Proceedings of Royal Society. Edinburgh*, Edinburgh, pp. 181–201.
- Hesp, P.A., 2002. Foredunes and blowouts: initiation, geomorphology and dynamics. *Geomorphology* 48, 245–268.
- Hesp, P.A., Walker, I.J., 2013. Coastal Dunes, in: Shroder, J.F., Lancaster, N., Sherman, D.J., Baas, A.C.W. (Eds.), *Treatise on Geomorphology*, Vol 11: Aeolian Geomorphology. Elsevier, San Diego, California, p. 439.
- Hesp, P.A., Smyth, T.A.G., Walker, I.J., Gares, P.A., Wasklewisz, T., 2016. Flow within a trough blowout at cape cod. *J. Coast. Res. Spec. Issue Coconut Creek Sl.* 288–292 <https://doi.org/10.2112/SI75-XXX.1>.

- Hilton, M., Nickling, B., Wakes, S., Sherman, D., Konlechner, T., Jermy, M., Geoghegan, P., 2017. An efficient, self-orienting, vertical-array, sand trap. *Aeolian Res.* 25, 11–21. <https://doi.org/10.1016/j.aeolia.2017.01.003>.
- Hotta, S., Horikawa, K., 1990. Function of sand fence placed in front of embankment. *Twenty-Second Coast. Eng. Conf.* 2754–2767.
- Hugenholz, C.H., Barchyn, T.E., 2011. Laboratory and field performance of a laser particle counter for measuring aeolian sand transport. *J. Geophys. Res. Earth Surf.* 116, 1–13. <https://doi.org/10.1029/2010JF001822>.
- Johannessen, J., MacLennan, A., 2007. *Beaches and Bluffs of Puget Sound and the Northern Straits Prepared in Support of the Puget Sound Nearshore Partnership*. Seattle, Washington.
- Keijser, J.G.S., De Groot, A.V., Riksen, M.J.P.M., 2015. Vegetation and sedimentation on coastal foredunes. *Geomorphology* 228, 723–734. <https://doi.org/10.1016/j.geomorph.2014.10.027>.
- Kennedy, D.M., Woods, J.L.D., 2012. The influence of coarse woody debris on gravel beach geomorphology. *Geomorphology* 159–160, 106–115. <https://doi.org/10.1016/j.geomorph.2012.03.009>.
- Komar, P.D., Rea, C.C., 1976. Erosion of Siletz spit. *Oregon. Shore & Beach* 44, 9–15.
- Lancaster, N., Baas, A., 1998. Influence of vegetation cover on sand transport by wind: Field studies at Owens Lake, California. *Earth Surf. Process. Landforms* 23, 69–82. [https://doi.org/10.1002/\(SICI\)1096-9837\(199801\)23:1<69::AID-ESP823>3.0.CO;2-G](https://doi.org/10.1002/(SICI)1096-9837(199801)23:1<69::AID-ESP823>3.0.CO;2-G).
- Li, B., Sherman, D.J., 2015. Aerodynamics and morphodynamics of sand fences: a review. *Aeolian Res.* 17, 33–48. <https://doi.org/10.1016/j.aeolia.2014.11.005>.
- Miot da Silva, G., Hesp, P., 2010. Coastline orientation, aeolian sediment transport and foredune and dunefield dynamics of Moçambique Beach, Southern Brazil. *Geomorphology* 120, 258–278. <https://doi.org/10.1016/j.geomorph.2010.03.039>.
- Nordstrom, K.F., Jackson, N.L., Klein, A.H.F., Sherman, D.J., Hesp, P.A., 2006. Offshore aeolian transport across a low foredune on a developed barrier island. *J. Coast. Res.* 225, 1260–1267. <https://doi.org/10.2112/06A-0008.1>.
- Nordstrom, K.F., Jackson, N.L., Hartman, J.M., Wong, M., 2007. Aeolian sediment transport on a human-altered foredune. *Earth Surf. Process. Landforms* 32, 102–115. <https://doi.org/10.1002/esp.1377>.
- Nordstrom, K.F., Jackson, N.L., Korotky, K.H., 2011. Aeolian sediment transport across beach wrack. *J. Coast. Res.* 59, 211–217. <https://doi.org/10.2112/SI59-022.1>.
- Ollerhead, J., Davidson-Arnott, R., Walker, I.J., Mathew, S., 2013. Annual to decadal morphodynamics of the foredune system at Greenwich Dunes, Prince Edward Island, Canada. *Earth Surf. Process. Landforms* 38, 284–298. <https://doi.org/10.1002/esp.3327>.
- Piscioneri, N., Smyth, T.A.G., Hesp, P.A., 2019. Flow dynamics over a foredune scarp. *Earth Surf. Process. Landforms*. <https://doi.org/10.1002/esp.4555>.
- Psuty, N.P., 1988. Sediment budget and dune/beach interaction. *J. Coastal Res.* 1–4. <https://doi.org/10.1007/soo382-012-1607-6>.
- Riegl, 2010. How to Generate a DTM in RiSCAN PRO [WWW Document]. URL <http://www.riegl.com/media-events/newsletter-archiv/1011-news-from-the-software-side-how-to-generate-a-dtm-in-riscan-pro/>
- Shepard, F.P., 1950. Beach Cycles in Southern California, Beach Erosion Board Technical Memorandum.
- Smyth, T.A.G., Jackson, D., Cooper, A., 2014. Airflow and aeolian sediment transport patterns within a coastal trough blowout during lateral wind conditions. *Earth Surf. Process. Landforms* 39, 1847–1854. <https://doi.org/10.1002/esp.3572>.
- Stemberger, J.E., 1979. Beach Protection Properties of Accumulated Driftwood, in: Proceedings of the Specialty Conference on Coastal Structures. US Army Corps of Engineers, Alexandria, Virginia, pp. 1052–1068.
- Stout, J.E., Zobeck, T.M., 1997. Intermittent saltation. *Sedimentology* 44, 959–970. <https://doi.org/10.1046/j.1365-3091.1997.d01-55.x>.
- Walker, I.J., Barrie, J.V., 2006. Geomorphology and sea-level rise on one of Canada's most sensitive coasts: Northeast Graham Island, British Columbia, in: *Journal of Coastal Research. Journal of Coastal Research*, Itajai, SC, Brazil, pp. 220–226.
- Wang, W., Zhao, W., Huang, L., Vimarlund, V., Wang, Z., 2014. Applications of terrestrial laser scanning for tunnels: a review. *J. Traff. Transp. Eng. (English Ed.)* 1, 325–337. doi:[https://doi.org/10.1016/S2095-7564\(15\)30279-8](https://doi.org/10.1016/S2095-7564(15)30279-8).
- Wheaton, J.M., Brasington, J., Darby, S.E., Sear, D.A., 2010. Accounting for uncertainty in DEMs from repeat topographic surveys: improved sediment budgets. *Earth Surf. Process. Landforms* 35, 136–156. <https://doi.org/10.1002/esp.1886>.
- Wolfe, S.A., Nickling, W.G., 1993. The protective role of sparse vegetation in wind erosion. *Prog. Phys. Geogr.* 17, 50–68. <https://doi.org/10.1177/03091339301700104>.